Tu N116 07

Converted Wave RTM Using Lowrank Wavefield Extrapolation

L. Casasanta* (CGG), Z. Xue (UT Austin) & S.H. Gray (CGG)

SUMMARY

Although wavefield extrapolation techniques are well developed for P-wave seismic imaging, ray based migration algorithms are still the workhorse for converted-wave (PS-wave) depth imaging. Full (exact) elastic-wave reverse-time anisotropic migration (RTM) has not been widely adopted for reasons of computational and workflow efficiency, despite its potential to deliver accurate sub-surface images in complex geological settings by directly solving the elastic wave equation. Even (approximate) converted-wave RTM in anisotropic media, using separate finite-difference propagators for quasi-P and quasi-S waves, is limited in applicability for algorithmic reasons. Here, we introduce an alternative converted-wave anisotropic RTM, using a low-rank decomposition of mixed-domain space-wavenumber propagators for quasi-P and quasi-S waves. These operators are formal integral solutions of the pure-mode wave equations which guarantee stable and dispersion-free time extrapolation for coarse time steps in anisotropic, heterogeneous media. The pure-mode extrapolators are attractive for both PS-wave structural imaging and velocity analysis. An ocean bottom cable synthetic example illustrates the effectiveness of low-rank PS-wave RTM when compared against state-of-the-art Gaussian beam and finite difference RTM algorithms.

Introduction

Wavefield extrapolation techniques are well developed for P-wave seismic imaging in anisotropic media, but multicomponent Kirchhoff migration remains the workhorse for converted-wave (PS-wave) depth imaging. Recently, Casasanta and Gray (2014) showed that PS-wave Gaussian-beam migration (GBM) improves both image quality and resolution by using: (1) better multipath book-keeping for velocity heterogeneity and S-wave anisotropy than single-arrival Kirchhoff migration; (2) localized coherent event de-noising. However, neither full elastic nor PS-wave reverse-time migration (RTM) has seen widespread use in practice, despite promising research over the last decade (Sun et al., 2006; Cheng et al. 2014). This is at least in part because popular finite difference (FD) solvers for both the elastic wave equation and (quasi-P and quasi-S, or qP and qS) wave equations suffer from both computational and algorithmic shortcomings.

From a computational standpoint, a fourth order FD stencil imposes either: dense grid spacing $((V_{S0}/f_{NYQ})/\max(\Delta x,\Delta y,\Delta z)\geq 2)$ for non-aliased slow $(V_{S0}\geq 100m/s)$ S-wave extrapolation; or small time steps $(V_{P0}\Delta t\sqrt{(1/\Delta x)^2+(1/\Delta y)^2+(1/\Delta z)^2}\leq 2\sqrt{3}/\pi)$ for stable fast $(V_{P0}\geq 1500m/s)$ P-wave propagation (Soubaras and Zhang, 2008). These constraints significantly increase the computational cost of both full elastic and PS-wave RTM compared to P-wave RTM. From an algorithmic standpoint, anisotropic elastic wave-extrapolators support the propagation of coupled P- and S-wave modes which must be separated at the image locations to avoid inter-modal cross-talk artefacts. Textbook elastic mode-decoupling (Yan and Sava, 2011) on a realistic 3D-survey is I/O intensive, as the operators involved are space-variant, and therefore memory "hungry". Although more efficient implementations are emerging (Cheng and Fomel, 2014), elastic wave mode separation still assumes accurate knowledge of the elastic-coefficient tensor, which is unlikely in early stages of depth imaging projects. Failure in wavefront separation will increase the amount of cross-talk noise, possibly to the point of questioning the advantages of full-wavefield imaging over ray-based imaging.

For anisotropic P-wave RTM, the standard propagator is a pseudo-acoustic FD solution of the elastic wave equation for transverse isotropic or orthorhombic media with arbitrarily oriented symmetry axis. In such media, S-wave velocity along the symmetry axis is set to zero $(V_{S0}=0)$, ensuring stable P-wave propagation in an energy bounded system as long as anisotropy parameters satisfy $\varepsilon\geq\delta$, and residual S-wave energy is generally weak and easy to remove before or after imaging. The analogous solution for anisotropic S-wave FD propagators is not applicable because the energy constraint for the pseudo-acoustic S-wave extrapolator requires $\varepsilon\leq\delta$ (Zhang et al., 2011).

To accommodate both qP and qS propagation in an accurate PS-wave RTM, we propose using mixed-domain (space/wavenumber) operators (Wards et al., 2008). These spectral operators implement analytical integral solutions of the scalar wave equations (Etgen and Brandsberg-Dahl, 2009; Fowler et al., 2010). These are suitable for PS-wave structural imaging and velocity analysis because they propagate pure-mode, dispersion-free qP- and qS-wavefields, and they are stable for large time steps, even (though impractical) beyond the Nyquist limit (Fowler et al., 2010). Further, the original space-wavenumber content of the wavefields is approximated to a desired accuracy by a lowrank decomposition (Fomel et al., 2013) which makes the wave-extrapolation feasible and accurate for practical application. We have implemented a PS-wave RTM using both one-step (Sun and Fomel, 2013) and two-step (Soubaras and Zhang, 2008) qP- and qSV- wave mixed-domain extrapolators using exact phase velocities in TI media. We present an ocean bottom cable (OBC) synthetic example to illustrate the effectiveness of this low-rank PS-wave RTM when compared against state of the art Gaussian beam (GBM) and pseudo-acoustic FD RTM algorithms in heterogeneous TTI media.

PS-wave extrapolation and lowrank approximation

Let $p(\mathbf{x},t)$ satisfy a scalar (P or S) wave equation in an inhomogeneous anisotropic medium described by its phase velocity $V(\mathbf{x},\mathbf{k})$, which depends on space $\mathbf{x}$ and wave vector $\mathbf{k}$. The wavefield at the next time step $t+\Delta t$ can be approximated by the mixed domain operator (Wards et al., 2008)

$$p(\mathbf{x},t+\Delta t)\cong\int d\mathbf{k}\, e^{i\phi(\mathbf{x},\mathbf{k},\Delta t)}\; P(\mathbf{k},t), \qquad (1)$$

where $P(\mathbf{k},t)$ is the spatial Fourier transform of the wavefield $p(\mathbf{x},t)$ at time step t and $\phi(\mathbf{x},\mathbf{k},\Delta t)$ is the mixed-domain phase function. In the high-frequency limit a second order Taylor expansion

approximates $\phi(\mathbf{x},\mathbf{k},\Delta t) \cong \mathbf{k}^T\mathbf{x} + V(\mathbf{x},\mathbf{k})[|\mathbf{k}|\Delta t + \nabla V(\mathbf{x},\mathbf{k})^T \mathbf{k}\,\Delta t^2/2]$ (Fomel et al., 2013). In continuous space, the stability of the recursion in equation 1 can be proved under a smoothness condition for phase velocity $V(\mathbf{x},\mathbf{k})$ for arbitrarily large time steps Δt (Ying and Sun,2014). Further, discretization of the method produces an unconditionally stable extrapolation for constant velocity $V(\mathbf{x},\mathbf{k}) = V(\mathbf{k})$. However, after spatial discretization, an analysis like that of Etgen (1994) is needed to assess the stability of the recursion in equation 1 for complicated subsurface models. Finally, two complex-valued one-step operators in equation 1 can be combined to obtain the real-valued two-step operator (Etgen and Brandsberg-Dahl, 2009; Soubaras and Zhang, 2008). The computational cost for a straightforward application of equation 1 is $O(N_{\mathbf{x}}^2)$, where $N_{\mathbf{x}}$ is the total size of the three-dimensional $\mathbf{x}$ grid. For fixed Δt, a lowrank r_ε approximation decomposes the wave extrapolation matrix into a separated representation with desired tolerance ε (Fomel et al., 2013):

$$W(\mathbf{x},\mathbf{k}) = e^{i[\phi(\mathbf{x},\mathbf{k},\Delta t) - \mathbf{k}^T\mathbf{x}]} \cong \sum_{m=1}^{M}\sum_{n=1}^{N} W(\mathbf{x},\mathbf{k}_m)\,a_{mn}\,W(\mathbf{x}_n,\mathbf{k}) \qquad (2)$$

Using representation 2, the computation in equation 1 corresponds to the evaluation of $M = N = r_\varepsilon$ inverse FFTs with a cost of $O(MN_{\mathbf{x}}\log N_{\mathbf{x}})$ per time step, where r_ε is generally a small number for the oscillatory kernel in equation 2. Differently from SVD, lowrank decomposition evaluates a set of N representative spatial location (rows) and M representative wavenumbers (columns) without requiring knowledge of the whole matrix in equation 2.

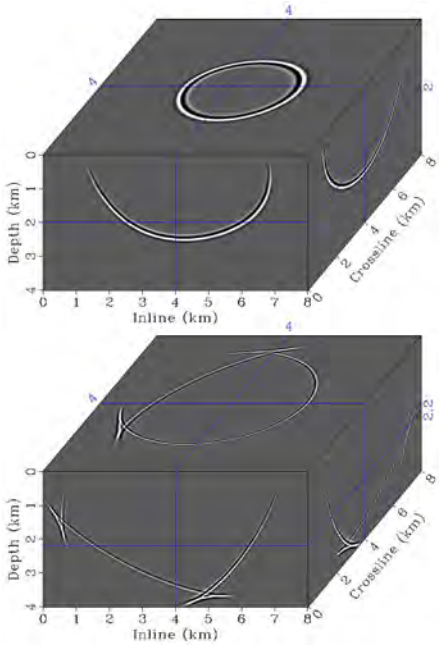

Figure 1: *Mixed-domain P- (a) and SV- (b) lowrank extrapolation snapshots in a constant 3D TI medium.* V_{P0}/V_{S0} =2.41, ε=.25, δ=.01, ϑ=30^0, φ=0^0.

Scalar PS-wave RTM requires the forward and backward time extrapolation of P- and S-wavefields injected at source and recording locations respectively. To this purpose we have designed mixed-domain P- and SV-wave matrices using equation 2 and the exact formulation for phase velocity $V(\mathbf{x},\mathbf{k})$ in a TI medium (Casasanta and Gray 2014):

$$2V_{P,SV}^2(\mathbf{x},\mathbf{k}) = V_{P0}^2\Big[2(1-f)|\mathbf{k}|^2 + f|\mathbf{k}|^2 + 2\varepsilon k_{r0}^2 \pm \sqrt{(f|\mathbf{k}|^2 + 2\varepsilon k_{r0}^2)^2 - 8f(\varepsilon-\delta)k_{n0}^2 k_{r0}^2}\Big] \qquad (3)$$

where δ and ε are Thomsen parameters and $f = 1 - V_{S0}^2/V_{P0}^2$ depends on qP- and qSV-wave velocities, the sign of the square root gives the qP- (+) or the qSV- (-) wave phase velocity. The normal $\mathbf{k}_{n0} = (\mathbf{k}^T\mathbf{c})\mathbf{c}$ and radial $\mathbf{k}_{r0} = \mathbf{k} - \mathbf{k}_{n0}$ wavenumbers are the $\mathbf{k}$ projection parallel and orthogonal to the symmetry axis $\mathbf{c}$. Figure 1 shows (a) qP- and (b) qSV-wavefield snapshots computed using a two-step lowrank wave extrapolator in a constant TI medium. The time-step size is Δt=5 ms and the spatial grid sizes in (*x*, *y*, *z*) are all Δ**x**=20 m for both qP- and qSV-wave extrapolation. Since the model is homogeneous, the rank is 1 for the lowrank decomposition. The qP-wavefield slices are anelliptical, and the qSV-wavefield accurately produces the triplication in the wave surface. Neither qP- nor qSV-wavefield contains coupled modes.

OBC synthetic example

We discuss image quality and computational performance achieved by lowrank PS-wave RTM using a 2D OBC synthetic dataset recorded on a sloping seafloor at approximately 1.2 km depth, with shots near the sea surface. Shot and receiver sampling are 25 m and 100 m, respectively. The subsurface structure is complex, including high shallow $V_{P0}/V_{S0} \sim 5$ and a salt body with rough topography (Figure 2). The medium is weakly anisotropic with a symmetry axis direction that follows the compaction trend. Figure 2 show the final stacked image obtained by using RTM based on our lowrank implementation of the one-step PS-wave extrapolators in equation 1. The input data spectrum

was limited to 20Hz. The grid spacings in (x, y, z) were equal. However, we used different grids to propagate the qSV- and qP-wavefields ($\Delta\mathbf{x}_S$=12.5m and $\Delta\mathbf{x}_P=2\Delta\mathbf{x}_S$) as well as different time steps ($\Delta t_S=2\Delta t_P$). In different experiments, we varied the length of the time step Δt_S from 2ms to 8ms while keeping the rank roughly the same ($M=N=18$), producing a range of errors in the lowrank approximation to equation 3. Figure 2 shows the results obtained using the least accurate approximation (i.e., largest error) for the mixed-domain qP- and qSV-wave matrix $W(\mathbf{x},\mathbf{k})$.

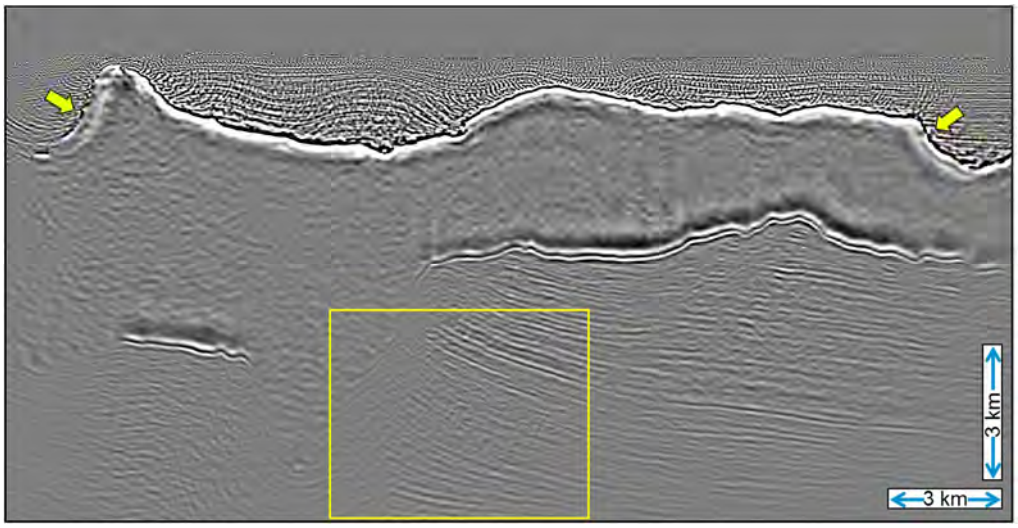

Figure 2 *OBC 2D synthetic PS-wave migration stack: one-step lowrank PS-wave RTM.*

We observed mild amplitude difference compared to the most accurate solution (smallest error) whilst the kinematics are essentially unaffected; the computation time gain was approximately a factor of two. Our lowrank RTM implementation (Figure 3c-f) generally outperforms the state-of-the art PS-wave GBM (Figure 3a-d) and quasi-acoustic FD RTM (Figure 3b-e) in the areas of interest. The steep shallow top of salt by our lowrank RTM (yellow arrows in Figure 2 and 3a-b-c) is more evident, although GBM shows cleaner sediments because of an imposed maximum-dip limitation of 70^0 which is missing in both FD and lowrank RTM. Conversely, GBM is unable to reproduce all the branches of the subsalt PS-wave propagation, and fails to image the deeper sediments as completely as RTM (Figure 3d). In the same area the FD RTM image (Figure 3e) is not as complete as the lowrank RTM image (Figure 3f). In fact, as we mentioned before, the qSV FD RTM extrapolator requires $\varepsilon \leq \delta$, which introduces an error in the S-wavefield kinematics away from the symmetry axis. This error is most evident on the steep shallow salt flanks and deeper subsalt sediments.

Conclusions

We have presented a novel PS-wave RTM implementation based on a lowrank approximation of the space-wavenumber mixed-domain wavefield extrapolator. Compared to FD RTM, the algorithm is attractive for scalar PS-wave imaging and velocity analysis because: (1) it is dispersion-free, with greater accuracy at high wavenumbers; (2) it is stable for large time steps, even beyond the Nyquist limit; (3) it propagates qP- and qS-waves with exact kinematics; (4) it offers direct control on the accuracy-efficiency trade-off by controlling the rank of the approximation in equation 3. Although investigations of stability and efficiency are ongoing, we speculate that RTM using lowrank wavefield extrapolation can become a technology of choice for high-fidelity PS-wave imaging.

Acknowledgements

We thank Chevron for providing the PS synthetic dataset. We also thank Sergey Fomel, Junzhe Sun, Botao Qin, Daniel Trad and Kristof De Meersman for stimulating discussions and critiques.

References

Casasanta, L., and Gray S. [2014], Converted-wave Gaussian-beam migration for sparse source or receivers: Geophysical Prospecting, *accepted for publication.*

Cheng, J., and Fomel, S, [2014], Fast algorithms of elastic wave mode separation and vector decomposition using low-rank approximation for anisotropic media : Geophysics, **79**, no. 4, C97–C110,

Cheng, J., Wu, Z., and Alkhalifah, T. [2014], Simulating propagation of decomposed elastic waves using low-rank mixed-domain integral operators for heterogeneous TI media: *84th Annual Meeting, SEG, Expanded Abstracts*, 3393-3399

Etgen, J., and Brandsberg-Dahl, S. [2009], The pseudo-analytical method: Application of pseudo-Laplacians to acoustic anisotropic wave propagation: *79th Annual Meeting, SEG, Expanded Abstracts*, 2552-2556.

Etgen , J. [1994] Stability of explicit depth extrapolation through laterally-varying media. SEG Technical Program Expanded Abstracts 1994,1266-1269.

Fomel, S., Ying, L., and Song, X. [2013], Seismic wave extrapolation using lowrank symbol approximation: Geophysical Prospecting, **61**, 526-536.

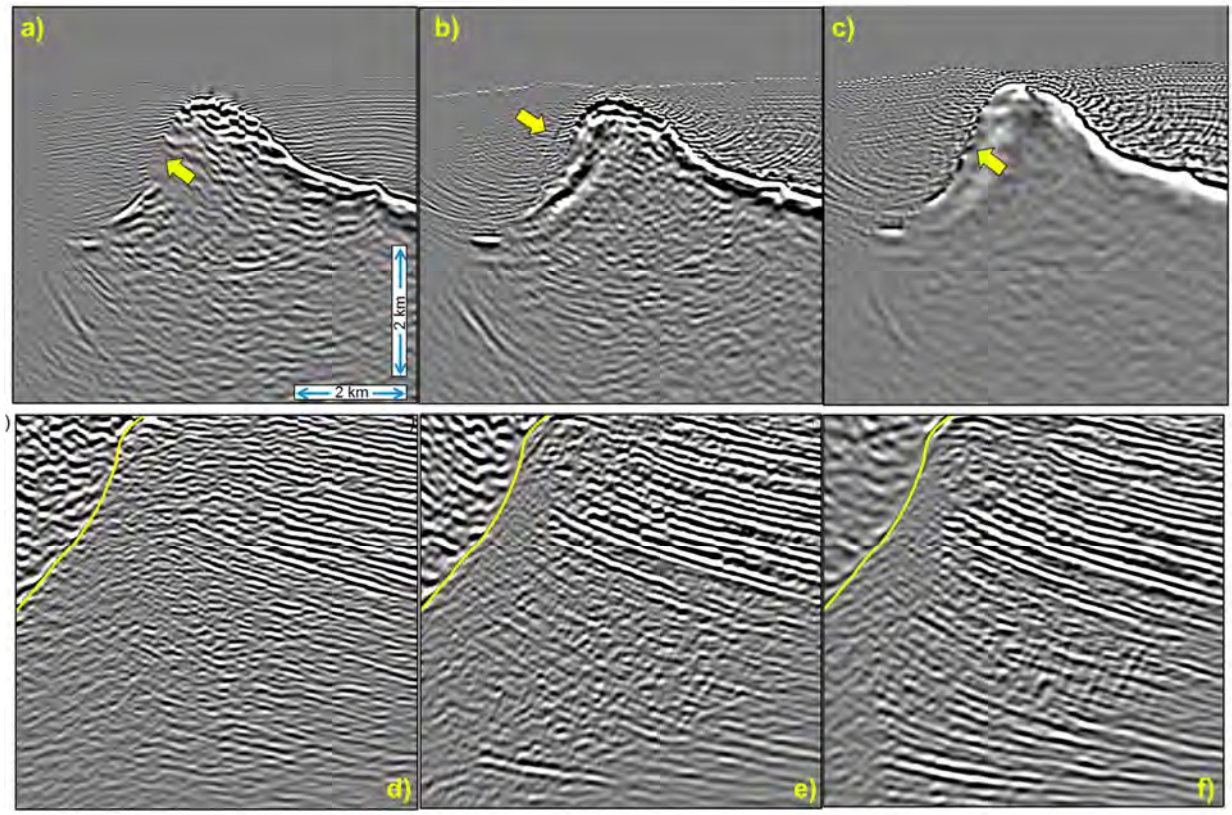

Figure 3 *OBC 2D synthetic PS-wave migration: CBM (a-b), FD RTM (c-d) and lowrank one-step RTM (e-f). (a-c-e): zoomed TOS in the left top corner of Figure 2. (b-d-f): zoomed subsalt sediment in the yellow square in Figure 2. The low-rank RTM results shows superior image quality and resolution particularly in the subsalt.*

Fowler, P. J., Du, X., and Fletcher, R.P., [2010b], Recursive integral time extrapolation methods for scalar waves: 80th Annual International Meeting, SEG, Expanded Abstracts, 3210–3215.

Sun, R., McMechan, Lee, G.A., Chow, C.J., and Chen. C., [2006]. Prestack scalar reverse-time depth migration of 3D elastic seismic data: Geophysics, **71**, S199-207.

Sun, J., and Fomel, S. [2013], Lowrank one-step wave extrapolation: *83rd Annual International Meeting, SEG, Expanded Abstracts*, 3905-3910.

Soubaras, R., and Zhang , Y., [2008], Two-step explicit marching method for reverse time migration: 78th Annual International Meeting, SEG, Expanded Abstracts, 2272-2276.

Wards, B.D., Margrave, G.F., and Lamoureux, M.P., [2010], Phase-shift time stepping for wavefield propagation: *80th Annual International meeting, SEG, Expanded Abstracts*, 2988-2992.

Yan, J., and Sava, P., [2011], Elastic wave-mode separation for TTI media: Geophysics, **76**, no. 4, T65-T78,

Ying, L., Y. and Sun, J. [2014], Personal communication.

Zhang, Y., Zhang, H., and Zhang, G, [2011]. A stable TTI reverse time migration and its implementation. Geophysics **76**, WA3-WA11.